

## ARTICLE OPEN

## Does elevation-dependent warming hold true above 5000 m elevation? Lessons from the Tibetan Plateau

Yanhong Gao<sup>1</sup>, Fei Chen<sup>2,3</sup>, Dennis P. Lettenmaier<sup>4</sup>, Jianwei Xu<sup>1</sup>, Linhong Xiao<sup>1</sup> and Xia Li<sup>1</sup>

Available observations below 5000 m altitude suggest that some mountain regions are undergoing accelerated elevation-dependent warming (EDW) in response to global or regional climate change. We address the question of whether EDW exists above 5000 m altitude, which is the elevation of much of the mountainous portion of the Tibetan Plateau, and headwaters to most of Asia's major rivers. We analyzed four data sources: in situ observations, gridded observations, ERA-Interim reanalysis, and Weather Research and Forecasting (WRF) regional climate model output over the portion of the Tibetan Plateau above 5000 m elevation. We also analyzed the relative contributions of changes in water vapor, diabatic heating, snow, and surface energy changes to EDW in WRF simulations and ERA-Interim. Gridded observations over the Tibetan Plateau show EDW below 5000 m, in apparent consistency with studies elsewhere. However, the gridded observations above 5000 m are essentially entirely extrapolated from lower elevations. Despite differences in details, neither ERA-Interim nor WRF indicate EDW above 5000 m. The WRF simulation produces more realistic temperature profiles at elevations where observations exist, which are also consistent with the simulated profiles of factors contributing to vertical heating. Furthermore, WRF projects no EDW above 5000 m in future climate projections (with CCSM4 boundary conditions) for RCP 4.5 and 8.5 global emission scenarios. Therefore, we conclude that EDW above 5000 m over the Tibetan Plateau is not occurring, nor is it likely to occur in future decades.

*npj Climate and Atmospheric Science* (2018)1:19; doi:10.1038/s41612-018-0030-z

## INTRODUCTION

Observations and modeling efforts for several mountain regions in the world indicate that greater surface warming occurs at higher altitudes.<sup>1–7</sup> Rangwala and Miller<sup>8</sup> examined elevation-dependent warming (EDW) over four mountain regions: the Swiss Alps, the Colorado Rocky Mountains, the Tibetan Plateau/Himalayas, and the Tropical Andes. They found that the available observations suggest that some mountain regions may be experiencing higher warming rates at seasonal time scales.

With mountain-peak elevations exceeding 8000 m, the Tibetan Plateau (TP) is an ideal place to examine mountainous EDW. Based on observations obtained from China Meteorological Administration (CMA) stations, a clear signal of EDW below 5000 m has been reported in recent decades over the TP.<sup>1–3,9</sup> Twenty-seven Global Climate Models (GCMs) in the Coupled Model Intercomparison Project phase 5 (CMIP5) also show increased rates of warming at high elevations in the Tibetan Plateau/Himalaya region in the twentieth century.<sup>10–12</sup> This phenomenon is projected to accelerate by the end of the twenty-first century under a high greenhouse gas emissions scenario.

In situ observations are typically considered to be ground truth in EDW analyses. However, the highest elevation in situ observations used in the EDW literature are about 5000 m (Table 1 in ref.<sup>8</sup>)—much lower than the elevation of the highest peak in Tibet (8848 m). Hence, whether EDW will affect the signature of climate change above 5000 m altitude remains largely uncertain. Regions above 5000 m altitude cover only 1/2000 of the global terrestrial

land area; however, about one-third of terrestrial average runoff originates in these areas. In fact, the glacier and snow meltwater from high elevations in the Tibetan Plateau/Himalaya region feed the headwaters of nine of Asia's major rivers including the Yangtze, Huang He (Yellow), Indus, Ganges, Brahmaputra, Irrawaddy, Salween, and Mekong Rivers. The headwaters of these rivers are all located above 5000 m and provide, in part or whole, the water source for approximately 10% of the world's population.<sup>13</sup> Lacking adequate observations, it is a challenge to assess whether these high-mountain headwater areas have warmed at a higher rate than the rest of the regional land surface. This has motivated the Mountain Research Initiative EDW working Group<sup>14</sup> to call for urgent attention to investigate potentially important changes in high-mountain environments in the global observational network.

In addition to in situ observations, studies of EDW have also employed gridded data interpolated from in situ station observations, data observed from satellites, atmospheric reanalyses, and global climate models. These data provide some information about EDW above 5000 m, but all have limitations.<sup>14</sup> For instance, gridded observations are generated using extrapolation of lower elevation in situ records. Satellite-based estimates have limited record lengths and often perform poorly at high altitudes.<sup>2,10,14–16</sup> Reanalysis data are not homogenized for climate trend analysis; and global climate models generally have poor spatial resolutions. Dynamical downscaling can bridge these gaps by providing continuous high-resolution information useful for high-elevation complex-terrain regions.<sup>9,17,18</sup> To address limitations arising from

<sup>1</sup>Key Laboratory of Land-surface Process and Climate Change in Cold and Arid Regions, Northwest Institute of Eco-environment and Resources, Chinese Academy of Sciences, Lanzhou, China; <sup>2</sup>National Center for Atmospheric Research, Boulder, CO 80301, USA; <sup>3</sup>State Key Laboratory of Severe Weather, Chinese Academy of Meteorological Sciences, China Meteorological Administration, Beijing, China and <sup>4</sup>Department of Geography, University of California Los Angeles, Los Angeles, CA, USA  
Correspondence: Yanhong Gao (gaoyh@lzb.ac.cn)

Received: 21 September 2017 Revised: 27 February 2018 Accepted: 26 March 2018

Published online: 03 October 2018

the sparseness of in situ stations in under-sampled high-altitude regions, the Mountain Research Initiative EDW working Group suggests the use of dynamically downscaling GCM simulations.<sup>14</sup> Motivated by the paucity of high-elevation observations, this is the primary approach we used here.<sup>9</sup>

## RESULTS

We analyzed warming rates over recent decades derived from four data sources: in situ observation, gridded observations,<sup>19</sup> ERA-Interim reanalysis,<sup>20</sup> and dynamical downscaling<sup>9</sup> of ERA-Interim using the Weather Research and Forecasting (WRF) model (see details in Data and Methods). Figure 1 shows the warming rates as a function of elevation divided into 500 m altitudinal bands starting from 2000 m. We found large discrepancies between inferred EDW among the different datasets. For instance, station records suggest EDW except for the elevations between 2000–3000 m and 4500–5000 m, while the gridded observations suggest a general EDW trend that does not agree with the station records for the elevations between 2000 and 3000 m. ERA-Interim shows a lower warming rate than the observations, agreeing with the gridded observation curve below 4000 m, but shows no EDW over Tibet above 4500 m. Following the EDW trend in the ERA-Interim boundary conditions, the results from WRF dynamical downscaling results do not show an EDW trend in the 2500–3500 m elevation range. However, in general the variations of warming in WRF as a function of elevation are more similar to gridded observations than to ERA-Interim itself.

More importantly, substantial differences in the warming rate derived from the gridded observations, ERA-Interim, and WRF are present above 5000 m. Gridded observations show a slight increasing trend above 5000 m, but both ERA-Interim and WRF show no continuous EDW above 5000 m. Furthermore, a continuous warming in the gridded observations above 5000 m is largely a result of extrapolation from lower elevation surface-station data. Interpolation is meaningful when there are measurement records that more or less span the range of elevations. However, the gridded observations, lacking station data above 5000 m, simply extrapolate observations from lower elevations. We believe therefore that apparent evidence of EDW above 5000 m based on gridded observations is spurious and misleading.

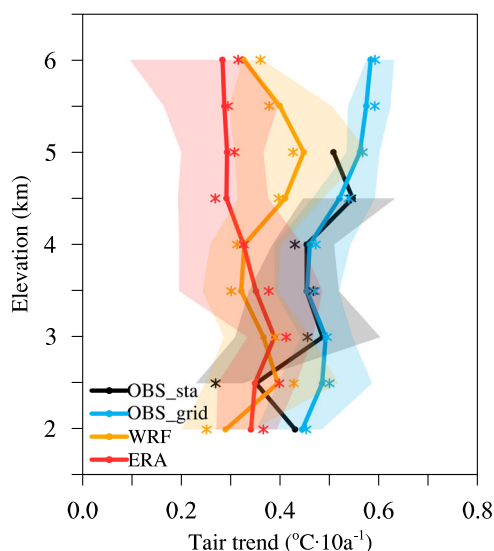


**Fig. 1** Observed and simulated mean (lines) and median (stars) surface air temperature linear trends for 1983–2011 vs. elevation bands with 500 m width. Spread is indicated with 25 and 75% percentiles in shades

In contrast, WRF output shows a decreasing warming rate above 5000 m, and ERA-Interim shows no EDW.

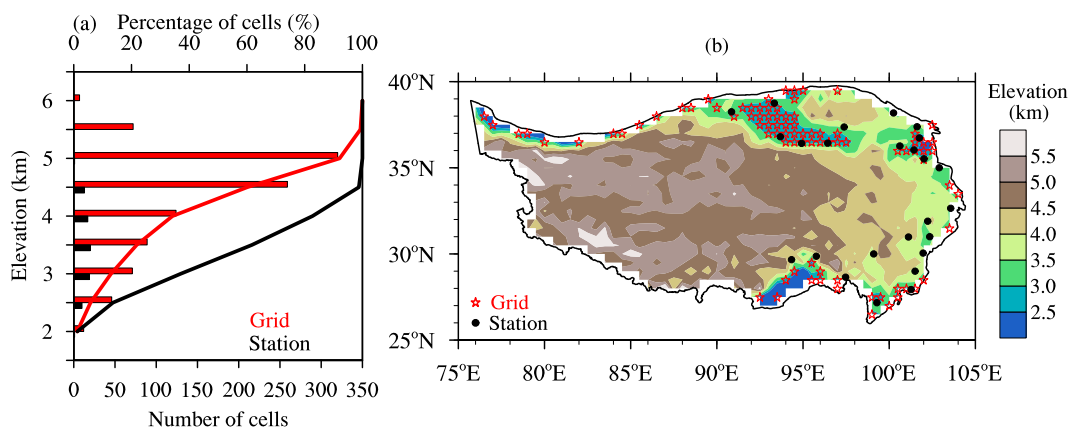
We focus first on the differences between station and gridded observations. Figure 2a shows a histogram of elevation in 500 m increments and the hypsometric curve for the Tibetan Plateau above 2000 m elevation based on the 0.5-degree spatial resolution gridded observations and station observations. There is a substantial difference between the topographic and station distributions: 60% of the grid cells have elevations between 4000 and 5000 m, but the majority of stations have elevations between 2000 and 4000 m, and only one station is in the 4500–5000 m elevation interval.

Figure 2b shows that stations between elevations 2000–3000 m are mostly scattered at the southeastern edge of Tibet in an area with steep terrain. All observation sites in these areas are located in valleys for the sake of accessibility and security of the equipment given the harsh environments and relief of the topography. To account for this bias in representation of elevations, the gridded surface air temperature was adjusted, by considering elevation differences between stations and smoothed grid cells, with a lapse rate that was estimated by a regression of the elevation and temperature at the stations.<sup>19</sup> Despite this, grid cells with 2000–3000 m elevations in the gridded dataset are actually located at the Chaidam basin (pentagons in Fig. 2b) rather than the southeastern edge of Tibet as a result of the smoothed topography resulting from the coarse 0.5-degree horizontal resolution used in the gridded observations.

Having established that there are no observations above 5000 m and the extrapolation beyond 5000 m in the gridded data likely is not reliable, we now focus on analyzing the physical processes that may contribute to differences in EDW between dynamical downscaling (WRF) and ERA-Interim below and above 5000 m. Physical processes, including snow-albedo feedback, changes in clouds and cloud properties, sensitivity of downward longwave radiation to specific humidity, and outgoing longwave radiation sensitivity to surface temperature, aerosols, and black carbon, have been identified as contributors to mountain EDW.<sup>8,14,21–23</sup> However, the interactions among those processes are complex and sometimes compensating.

Figure 3 shows linear trends in tropospheric water vapor and diabatic heating release averaged over three pressure levels (300, 400, and 500 hPa), snow-water equivalent (SWE), snowfall (Snow), and precipitation (Prec) vs. elevation bands with 500 m width for ERA-Interim and WRF simulations for 1983–2011. As for the specific humidity contribution, Fig. 3a shows that both ERA-Interim and WRF exhibit maximum intensified moisture at 5000 m, which partly explains the maximum EDW at 5000 m in the WRF results,<sup>14,21–23</sup> but does not explain the maximum EDW at 3000 m in ERA-Interim. Although warming is not proportional to intensified moisture due to the non-linear relationship between specific humidity and downwelling longwave radiation, the EDW in WRF below 5000 m is consistent with its moisture variations and arguably is more realistic than that in ERA-Interim. Moreover, Fig. 3b shows that WRF predicts an enhanced diabatic heating release starting from 3500 m with a maximum at 5000 m, which again is consistent with its EDW vertical profile. There is no diabatic heating output in ERA-Interim. Usually, the diabatic heating is closely correlated with water vapor as the WRF results show. Therefore, we infer that the diabatic heating in ERA-Interim shows a similar profile with water vapor, which does not explain the EDW in ERA-Interim.

We consider the snow-albedo feedback to be the dominant influence based on previous studies (such as 8) that show its effect in mountainous regions with snowpack wherever the snowline is receding. Results from ERA-Interim and WRF are self-consistent regarding the snow-albedo feedback mechanism. Over Tibet, tree lines are located around 4000–4300 m with alpine meadows above the tree line but below 5000 m.<sup>24</sup> Above 5000 m, glacier



**Fig. 2** **a** Histogram of elevation in 500 m interval and hypsometric curve for the Tibetan Plateau (over 2000 m) based on the 0.5-degree resolution elevation and observation stations. Solid lines represent the number and the percentage of cells/stations below a given threshold. **b** Topography of 0.5-degree resolution grid cells over the TP (shades) and locations of stations and grid cells with elevations at 2000–3000 m: stations in dots and grid cells in pentagons

and snow cover much of the bare ground most of the year. The thickness and stability of the glaciers and snowpack increase with elevation and lower surface air temperature. Stable snowpacks exist above about 6000 m.<sup>24</sup> In the vicinity of 5000 m elevation, the surface cover transitions from a mix of alpine meadows and seasonal snow cover to a mix of bare ground covered with glaciers and snowpack, leading to an increased surface albedo relative to the lower elevation transition zone. As the climate warms, Fig. 3c shows an increased snowpack melt in WRF at low elevations, especially below 5000 m where there is mixed vegetation, leading to lower albedo. Above 5000 m, increased snowfall in a warmer climate (Fig. 3d) partially compensates for increased snowmelt and as a result there is little change in albedo. Reduced surface albedo below 5000 m results in greater absorption of downward solar radiation at the surface and further enhances the warming and snow melt, accelerating the positive feedback between snowmelt and surface warming. Hence, a maximum SWE reduction occurs around the elevation of about 5000 m (Fig. 3c). In contrast to the WRF results, ERA-Interim does not produce enhanced SWE reduction over Tibet, and has no EDW above 3000 m.

Besides melting, snowpack reduction could result from sublimation or snowfall decreases. However, neither WRF nor ERA-Interim show evidence of increased surface wind speed, hence no tendency for increased snow sublimation. Therefore, the snowpack reduction is mainly driven by increased net radiation as a result of lower albedo, which we discuss further below. ERA-Interim and WRF both produce increased precipitation from 2500 m up to 6000 m with a maximum increase around 5000 m (Fig. 3e), suggesting a general wetting trend over Tibet, consistent with previous reports.<sup>25–27</sup> However, such an increase in precipitation does not translate into a proportional increase in snowfall. For instance, the negative snowfall linear trends below 4500 m in ERA-Interim and WRF result from less snowfall being partitioned from total precipitation as a response to warming.<sup>28</sup> Above 4500 m, snowfall in ERA-Interim continues to decrease due to its coarse resolution, smoothed topography, and deficiency in the underlying model's representation of snow processes.<sup>29</sup> However, WRF simulates increased snowfall as a result of more precipitation at higher elevation and air temperature below the freezing point. This result is largely consistent with WRF simulations in the Colorado headwaters.<sup>18</sup> Therefore, the elevated warming rather than sublimation or reduced snowfall seems to be the key factor for SWE reductions above 4000 m.<sup>11</sup>

To further illustrate the snow-albedo feedback contribution to warming rate in WRF and ERA-Interim above 5000 m, Fig. 4 compares spatial distributions of warming rates, SWE linear trends,

surface latent heat flux changes, sensible heat flux changes, and surface net radiation changes for both WRF (left) and ERA-Interim (right). In the left panels, the WRF simulation shows the highest warming rate over the Tanggula ranges (Fig. 4a). Even though the Himalaya and Kalakunlun ranges in the southwest and northwest have higher peak elevations, the warming rates for these two mountain ranges are less than those for the Tanggula range with average elevation (around 5000 m at 0.5-degree horizontal resolution). This warming pattern is consistent with the observed SWE-change patterns (Fig. 4b) and glacier-change patterns over Tibet: a more substantial retreat in Tanggula which has a lower elevation and relatively higher temperatures, whereas glacier extents have increased in the Kalakunlun ranges with higher elevations and colder temperatures.<sup>30,31</sup> Furthermore, our computed changes in net radiation and sensible and latent heat fluxes (Fig. 4c–e) are consistent with the contrasting warming signals and SWE reduction between the Kalakunlun and Tanggula ranges. A large part of the increased net radiation is partitioned into sensible heat over the Tanggula ranges, but into latent heat flux over the Kalakunlun ranges. Higher sensible heat flux over the Tanggula range as compared with the Kalakunlun Mountains (Fig. 4d) helps raise the surface air temperature in spring, resulting in more melting of snowpack and glaciers at 5000 m than above (Figs. 4b and 3c).

On the other hand, in the right panels of Fig. 4, ERA-Interim shows smaller SWE decreases compared to WRF (Fig. 4g). SWE reductions in ERA-Interim occur in the west of the Kalakunlun range, but there are increases in the Tanggula range. Larger SWE reductions in the Kalakunlun range cause decreases in the surface latent heat fluxes and increases in the sensible heat fluxes. In contrast, positive trends in latent heat fluxes and negative trends in sensible heat fluxes are found in the Tanggula range. ERA-Interim shows more or less uniform depressions in surface net radiation fluxes (Fig. 4j) above 5000 m (in contrast to increases in WRF), leading to no EDW (Fig. 4f).

Finally, we also explored future changes in EDW using WRF downscaled projections using boundary conditions from CCSM4. In these projections, surface air temperature increases 1.0–1.5 °C in the near future (2016–2035) under Representative Concentration Pathway (RCP) scenarios 4.5 and 8.5.<sup>32</sup> Our results show the greatest warming at 5000 m, which is the same as the elevation of the maximum in the past period (Fig. 5). CCSM4 also shows an EDW with warming of 1.0–1.2 °C in the near future (2016–2035) with a similar warming profile at a maximum of 5000–5500 m. By the end of this century (2080–2100), warming increases 2–3 times when compared with the near future, especially under RCP 8.5. Consistent with the historical and near future periods, WRF

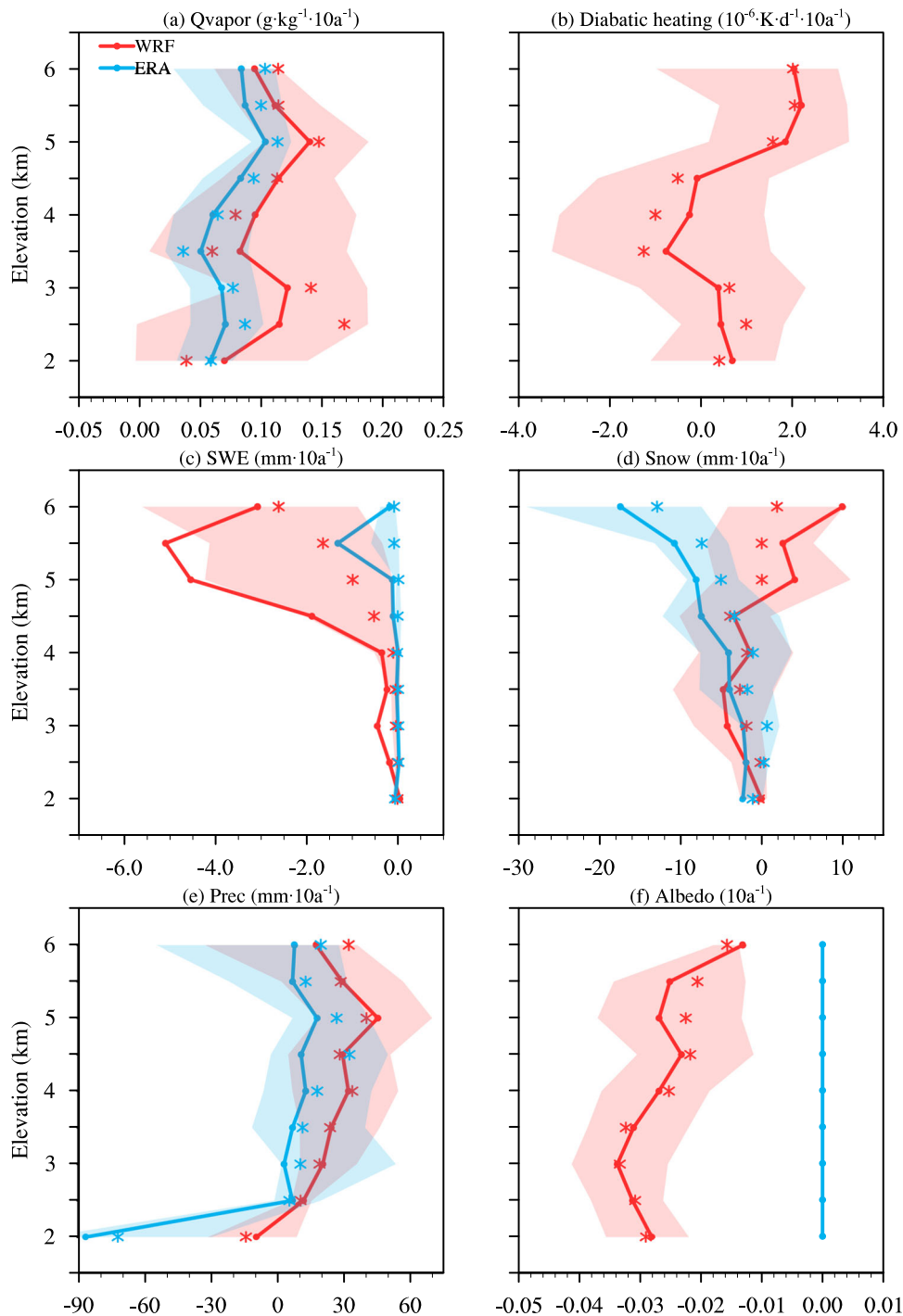


**Fig. 3** Mean (lines) and median (stars) linear trends of simulated annual mean **a** vertical averaged tropospheric water vapor, **b** vertical averaged tropospheric diabatic heating releasing, **c** snow-water equivalent, **d** snowfall, **e** precipitation, and **f** albedo in April vs. elevation bands with 500 m width for ERA-Interim and WRF simulation in 1983–2011. Spread is indicated with 25 and 75% percentiles in shades

projects EDW below 5000 m and reverses above. CCSM4 projects less warming than WRF and with no apparent EDW. In summary, we do not find evidence of EDW above 5000 m occurring in either future WRF projections (RCP 4.5 and 8.5) or in the underlying CCSM4 simulation by the end of this century. The reason for the lack of EDW in future projections is unclear (one might expect EDW as temperatures rise due to reduced snow cover, and snow-albedo feedback as discussed above), and needs to be explored in future work. One possible explanation might be differential current-climate temperature simulations between the WRF and

CCSM4 runs and observations. CCSM4 underestimates surface air temperature by 2–6 °C (relatively uniformly with elevation); WRF simulates a more elevation-dependent temperature and exhibits colder temperature above 5000 m than CCSM4 because of more aggressive representation of elevation variations. Hence, the 2–4 °C future warming may not be sufficient to shift the current maximum snow-albedo feedback at around 5000 m to higher elevations in the future projections. Given that there are no stations above 5000 m and the WRF simulations are closer to observations (than CCSM4) below 5000 m where there are



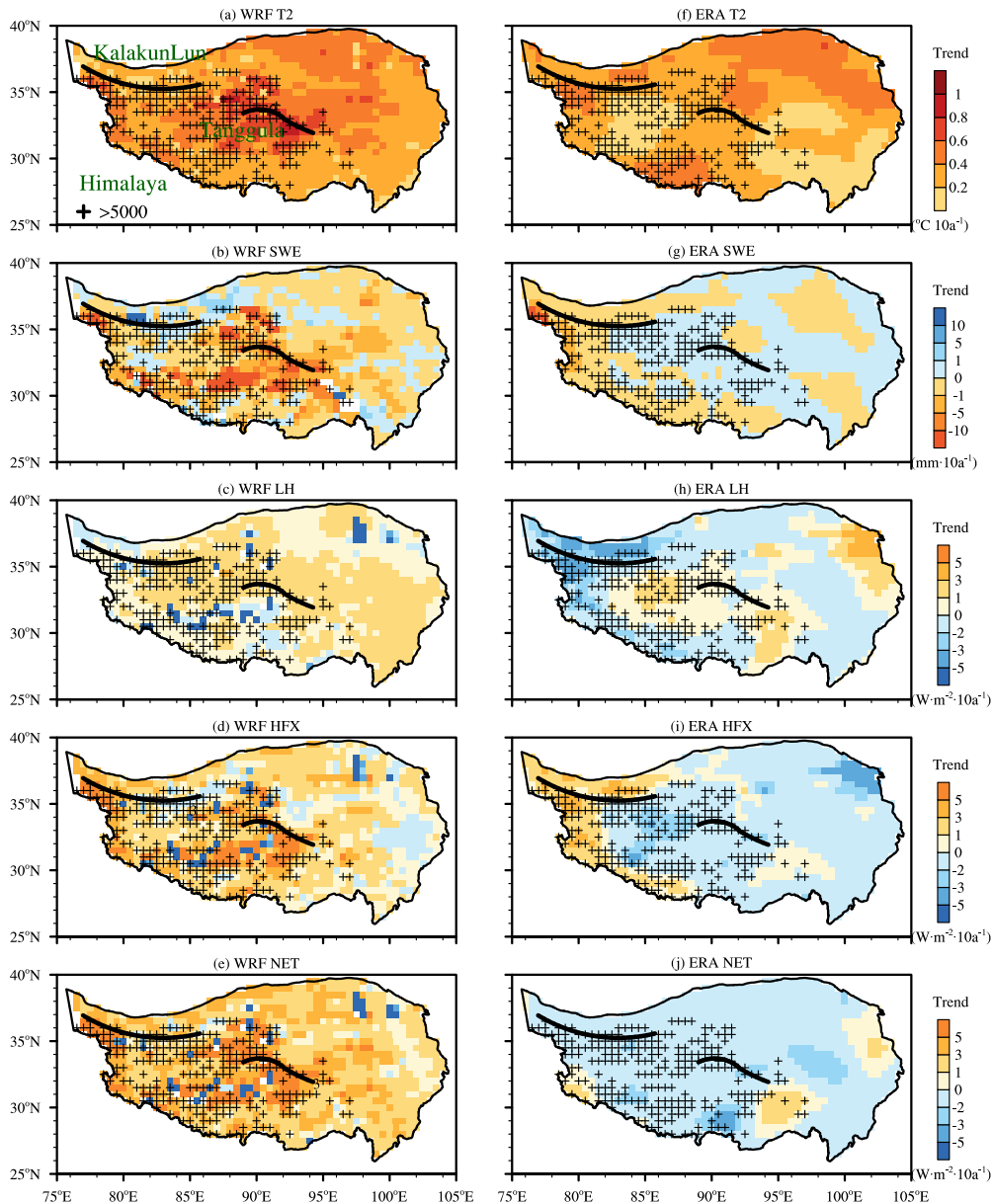


**Fig. 4** Distribution of WRF simulated **a** surface air temperature linear trends, **b** SWE linear trends, **c** surface latent heat flux changes, **d** sensible heat flux changes, and **e** surface net radiation changes. (**f–j**) Are the same as (**a–e**) but for ERA-Interim in 1983–2011. Grid cells for elevations above 5000 m are labeled as pluses. Kalakunlun (NW) and Tanggula (SE) ranges are marked as black

observations, we are inclined to place more stock in the WRF simulations.

## DISCUSSION

We analyzed four datasets to evaluate EDW above 5000 m over the Tibetan Plateau, where observation stations are essentially nonexistent. Our main findings are:

1. In situ stations show EDW below 5000 m over the period 1983–2011. Gridded observations generally follow the in situ records below 5000 m where most of the stations lie. ERA-Interim reanalysis underestimates the station-based warming rate and does not have an EDW signal above 3000 m. The WRF results follow the observed EDW curve below 5000 m, but with lower warming rates than observations, likely inherited from the ERA-Interim boundary conditions.

2. There are large discrepancies in warming estimates above 5000 m where no in situ stations exist. Gridded observations show EDW based on station extrapolation. Despite differences in details, neither WRF nor ERA-Interim suggest EDW above 5000 m.
3. WRF and ERA-Interim are consistent regarding the snow-albedo feedback mechanism, albeit their EDW rates differ. Water vapor changes and diabatic heating releases contribute to EDW in WRF, but have no effect in ERA-Interim.
4. Future WRF runs (with CCSM4 boundary conditions) also project a maximum warming rate at about 5000 m that reverses above 5000 m under RCP 4.5 and 8.5 in both the near and long terms.

Based on these findings, we conclude that EDW above 5000 m over the Tibetan Plateau is not occurring, nor is it likely to occur in the future.

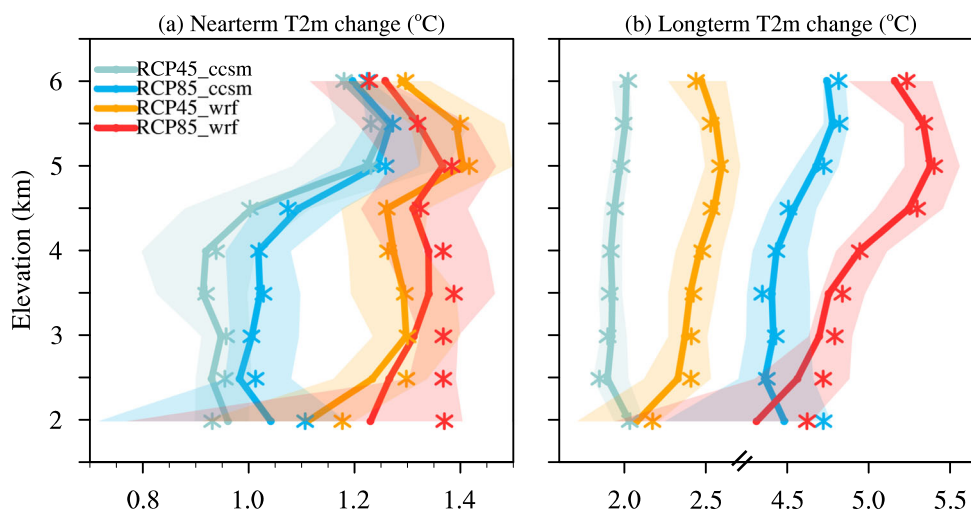


**Fig. 5** Mean and median projections of CCSM4 and WRF simulated surface air temperature changes vs. elevation bands with 500 m width (unit: km) for **a** near-term (2016–2035) and **b** long-term (2080–2100) futures under the Representative Concentration Pathway (RCP) scenarios 4.5 and 8.5. Spread is indicated with 25 and 75% percentiles in shades

## METHODS

We are not aware of any research-quality temperature observations available over the TP above 5000 m, which motivated our use of ERA-Interim and WRF as our primary information sources. The ERA-Interim reanalysis ranks the best among the examined four reanalyses in describing temperature and elements of the water cycle over the TP.<sup>26</sup> The period of record for ERA-Interim is 1979–present. We conducted WRF version 3.3 simulations using ERA-Interim boundary conditions for the period 1979–2011 with a horizontal resolution of 30 km, using the NCAR Community Atmospheric Model (CAM) shortwave and longwave schemes, Single-Moment 3-class (WSM3), Grell–Devenyi convection scheme, Yonsei University planetary boundary layer (YSU PBL), and the Noah land surface model. We took the first four years (1979–1982) of our model run as spin-up; 4 years is sufficient for initialization of soil moisture and other land-state variables based on our previous experience.<sup>33,34</sup> The common period after spin-up (1983–2011) was used in our linear trend calculations.

For our comparisons of EDW below 5000 m, we used raw station observations, as well as gridded observations from the National Meteorological Information Center of the CMA. CMA compiled the dataset using thin-plate-spline interpolation<sup>19</sup> and land information from stations.

We compared precipitation, SWE, snowfall, and surface heat fluxes from ERA-Interim and WRF. We also analyzed the water vapor and diabatic heating output from these two sources. Diabatic heating may include contributions from model physics such as PBL for surface heating, radiation, convection, and microphysics. It is the sum of tendencies of the physics schemes. However, in WRF, diabatic heating is from microphysics alone. The influence of water vapor on downwelling radiation depends on the atmospheric column above the station. Using a single level is not sufficient to represent the water vapor influences, in particular on downwelling longwave radiation. Therefore, given that the water vapor is mainly confined in the troposphere below 300 hPa, to represent water vapor variations with elevation, for each model grid point, we first calculated the trend in water vapor and diabatic heating at 300, 400, and 500 hPa, respectively. We then averaged the trends over the three levels to represent general variations in tropospheric water vapor and diabatic heating (we only include 500 hPa when this level is above the surface; otherwise we average 300 and 400 hPa).

For each gridded dataset, we then binned the results by elevation bands in 500 m increments, starting at 2000 m. We analyzed station and grid cell mean and median warming rates and plotted them (in Figs. 1, 3, and 5). We used the 25th and 75th percentile grid values for each elevation band to characterize the spread.

## Code availability

All figures were produced by NCL 6.4.0; the code is available from the authors

## Data availability

All data used in this paper are available from the authors

## ACKNOWLEDGEMENTS

The reanalysis output used in this study were provided by the Research Data Archive (RDA) which is maintained by the Computational and Information Systems Laboratory (CISL) at the National Center for Atmospheric Research (NCAR). The in situ station and gridded observations were provided by the National Climate Center of CMA. We thank the Super-Computing Center of the Chinese Academy of Science for computational resources. This research was jointly supported by the Strategic Priority Research Program of Chinese Academy of Sciences (XDA2006010202), the National Natural Science Foundation of China (91537211, 91537105), and the National Center for Atmospheric Research Water System Program.

## AUTHOR CONTRIBUTIONS

Y.G. designed the study and conducted the WRF simulations. L.X., X.L., and J.X. analyzed the data and plotted the figures. Y.G., F.C., and D.P.L. contributed to the writing, especially of revisions and content added to respond to review comments.

## ADDITIONAL INFORMATION

**Competing interests:** The authors declare no competing interests.

**Publisher's note** Springer Nature remains neutral with regard to jurisdictional claims in published maps and institutional affiliations.

## REFERENCES

- Liu, X., Cheng, Z., Yan, L. & Yin, Z. Elevation dependency of recent and future minimum surface air temperature trends in the Tibetan Plateau and its surroundings. *Glob. Planet. Change* **68**, 164–174 (2009).
- Qin, J., Yang, K., Liang, S. & Guo, X. The altitudinal dependence of recent rapid warming over the Tibetan Plateau. *Clim. Change* **97**, 321–327 (2009).
- Rangwala, I., Miller, J. & Xu, M. Warming in the Tibetan Plateau: possible influences of the changes in surface water vapor. *Geophys. Res. Lett.* **36**, L06703 (2009).
- Zubler, E. M. et al. Localized climate change scenarios of mean temperature and precipitation over Switzerland. *Clim. Change* **125**, 237–252 (2014).
- Gilbert, A. & Vincent, C. Atmospheric temperature changes over the 20th century at very high elevations in the European Alps from englacial temperatures. *Geophys. Res. Lett.* **40**, 2102–2108 (2013).
- Rangwala, I. & Miller, J. R. Twentieth century temperature trends in Colorado's San Juan Mountains. *Arct. Antar. Alp. Res.* **42**, 89–97 (2010).

7. Diaz, H. F. & Bradley, R. S. Temperature variations during the last century at high elevation sites. *Clim. Change* **36**, 253–279 (1997).
8. Rangwala, I. & Miller, J. R. Climate change in mountains: a review of elevation-dependent warming and its possible causes. *Clim. Change* **114**, 527–547 (2012).
9. Gao, Y., Xu, J. & Chen, D. Evaluation of WRF mesoscale climate simulations over the Tibetan Plateau during 1979–2011. *J. Clim.* **28**, 2823–2841 (2015).
10. Palazzi, E., Filippi, L. & Hardenberg, J. V. Insights into elevation-dependent warming in the Tibetan Plateau-Himalayas from CMIP5 model simulations. *Clim. Dyn.* **48**, 3991–4008 (2017).
11. Rangwala, I., Sinsky, E. & Miller, R. J. Amplified warming projections for high altitude regions of the Northern hemisphere mid-latitudes from CMIP5 models. *Environ. Res. Lett.* **8**, 024040 (2013).
12. Rangwala, I., Sinsky, E. & Miller, R. J. Variability in projected elevation dependent warming in boreal midlatitude winter in CMIP5 climate models and its potential drivers. *Clim. Dyn.* **46**, 2115–2122 (2016).
13. Schaner, N., Voisin, N., Nijssen, B., & Lettenmaier, D. P.. The contribution of glacier melt to streamflow. *Environ. Res. Lett.* **7**, 1–8 (2012).
14. Pepin, N., Bradley, R.S., Diaz, H.F., Baraer, M., Caceres, E.B., Forsythe, N., Fowler, H., Greenwood, G., Hashmi, M.Z., Liu, X.D., Miller, J.R., Ning, L., Ohmura, A., Palazzi, E., Rangwala, I., Schöner, W., Severskiy, I., Shahgedanova, M., Wang, M.B., Williamson, S.N., Yang, D.Q. Elevation-dependent warming in mountain regions of the world. *Nat. Clim. Change* **5**, 424–430 (2015).
15. Shamir, E. & Georgakakos, K. P. MODIS land surface temperature as an index for surface air temperature for operational snowpack estimation. *Remote Sens. Environ.* **152**, 83–98 (2014).
16. Pepin, N. C., Maeda, E. E. & Williams, R. Use of remotely-sensed land surface temperature as a proxy for air temperatures at high elevations: findings from a 5,000 metre elevational transect across Kilimanjaro. *J. Geophys. Res. Atmos.* **121**, 9998–10015 (2016).
17. Gao, Y., Vano, J. A., Zhu, C. & Lettenmaier, D. P. Evaluating climate change over the Colorado River basin using regional climate models. *J. Geophys. Res.* **116**, D13104 (2011).
18. Rasmussen, R. et al. Climate change impacts on the water balance of the Colorado headwaters: high-resolution regional climate model simulations. *J. Hydrometeorol.* **15**, 1091–1116 (2014).
19. Xu, Y. et al. A daily temperature dataset over China and its application in validating a RCM simulation. *Adv. Atmos. Sci.* **26**, 763–772 (2009).
20. Simmons, A., Uppala, S., Dee, D. & Kobayashi, S. ERA-Interim: new ECMWF reanalysis products from 1989 onwards. *ECMWF Newsl.* **110**, 25–35 (2006).
21. Lau, W., Kim, M., Kim, K. & Lee, W. Enhanced surface warming and accelerated snow melt in the Himalayas and Tibetan Plateau induced by absorbing aerosols. *Environ. Res. Lett.* **5**, 025204 (2010).
22. Rangwala, I., Miller, J. R., Russell, G. L. & Xu, M. Using a global climate model to evaluate the influences of water vapor, snow cover and atmospheric aerosol on warming in the Tibetan Plateau during the twenty-first century. *Clim. Dynam.* **34**, 859–872 (2010).
23. Yan, L., Liu, Z., Chen, G., Kutzbach, J. E. & Liu, X. Mechanisms of elevation-dependent warming over the Tibetan plateau in quadrupled CO2 experiments. *Clim. Change* **135**, 509–519 (2016).
24. Shi, Y., Huang, M., Yao, T. & Deng, Y. *Glaciers and Their Environments In China – The Present, Past and Future* (Science Press, Beijing, 2000).
25. Gao, Y., Leung, L. R., Zhang, Y. & Lan, Cuo Changes in moisture flux over the Tibetan Plateau during 1979–2011: insights from the high-resolution simulation. *J. Clim.* **28**, 4185–4197 (2015).
26. Gao, Y., Cuo, Lan & Zhang, Y. Changes in moisture flux over the Tibetan Plateau during 1979–2011 and possible mechanisms. *J. Clim.* **27**, 1876–1893 (2014).
27. Gao, Y., Li, X., Leung, R. L., Chen, D. & Xu, J. Aridity changes in the Tibet Plateau in a warming climate. *Environ. Res. Lett.* **10** 034013, 3 (2015).
28. O’Gorman, P. A. Contrasting responses of mean and extreme snowfall to climate change. *Nature* **512**, 416–418 (2014).
29. Su, F., Duan, X., Chen, D., Hao, Z. & Cuo, L.. Evaluation of the global climate models in the CMIP5 over the Tibetan Plateau. *J. Clim.* **26**, 3187–3208 (2013).
30. Yao, T. et al. Different glacier status with atmospheric circulations in Tibetan Plateau and surroundings. *Nat. Clim. Change* **2**, 663–667 (2012).
31. Kapnick, S., Delworth, T., Ashfaq, M., Malyshev, S. & Milly, P. C. D. Snowfall less sensitive to warming in Karakoram than in Himalayas due to a unique seasonal cycle. *Nat. Geosci.* **7**, 834–840 (2014).
32. Gao, Y., Xiao, L., Chen, D., Xu, J. & Zhang, H. Comparison between past and future extreme precipitations simulated by global and regional climate models over the Tibetan Plateau. *Int. J. Climatol.* **38**, 1285–1297 (2018).
33. Gao, Y., Li, K., Chen, F., Jiang, Y. & Lu, C. Assessing and improving Noah-MP land model simulations for the central Tibetan Plateau. *J. Geophys. Res. Atmos.* **120**, 9258–9278 (2015).
34. Gao, Y. et al. Quantification of the relative role of land surface processes and large scale forcing in dynamic downscaling over the Tibetan Plateau. *Clim. Dyn.* **48**, 1705–1721 (2016).



**Open Access** This article is licensed under a Creative Commons Attribution 4.0 International License, which permits use, sharing, adaptation, distribution and reproduction in any medium or format, as long as you give appropriate credit to the original author(s) and the source, provide a link to the Creative Commons license, and indicate if changes were made. The images or other third party material in this article are included in the article’s Creative Commons license, unless indicated otherwise in a credit line to the material. If material is not included in the article’s Creative Commons license and your intended use is not permitted by statutory regulation or exceeds the permitted use, you will need to obtain permission directly from the copyright holder. To view a copy of this license, visit <http://creativecommons.org/licenses/by/4.0/>.

© The Author(s) 2018